

Characterization of 3-D coronary tree motion from MSCT angiography

Guanyu Yang^{1 2 3}, Jian Zhou^{1 2 3}, Dominique Boulmier^{1 4}, Marie-Paule Garcia^{1 2}, Limin Luo^{2 3}, Christine Toumoulin^{1 2 *}

¹ LTSI, Laboratoire Traitement du Signal et de l'Image INSERM : U642, Université de Rennes I, Campus de Beaulieu, 263 Avenue du Général Leclerc - CS 74205 - 35042 Rennes Cedex, FR

² CRIBS, Centre de Recherche en Information Biomédicale sino-français INSERM : Laboratoire International Associé, Université de Rennes I, SouthEast University, Nankin, CN

³ LIST, Laboratory of Image Science and Technology SouthEast University, Si Pai Lou 2, Nanjing, 210096, CN

⁴ Département de cardiologie et maladies vasculaires CHU Rennes, Hôpital Pontchaillou, Université de Rennes I, 2 rue Henri Le Guilloux 35033 RENNES cedex 9, FR

* Correspondence should be addressed to: Christine Toumoulin <christine.toumoulin@univ-rennes1.fr >

Abstract

This paper describes a method for the characterization of coronary artery motion using Multi-slice Computed Tomography (MSCT) volume sequences. Coronary trees are first extracted by a spatial vessel tracking method in each volume of MSCT sequence. A point-based matching algorithm, with feature landmarks constraint, is then applied to match the 3D extracted centerlines between two consecutive instants over a complete cardiac cycle. The transformation functions and correspondence matrices are estimated simultaneously and allow deformable fitting of the vessels over the volume series. Either point-based or branch-based motion features can be derived. Experiments have been conducted in order to evaluate the performance of the method with a matching error analysis.

Author Keywords Centerline extraction ; coronary tree ; 3-D motion ; multislice computed tomography (MSCT) angiography ; pointbased matching.

Introduction

Cardiac diseases remain a leading cause of mortality in Europe and in the US [1]. Quantitative and accurate characterization of abnormal wall and vascular patterns (location, shape, motion) of the heart is thus of major importance for diagnosis and treatment [2]. For a long time, the mono- and bi-plane X-ray techniques were only available to deal with coronary and ventricular structures. Pioneering attempts, mainly focused on static reconstruction, were thus based on computer vision approaches relying on epipolar techniques and feature matching. A first coupled reconstruction-motion estimation was proposed in [3] and led to a fast and efficient scheme to recover the centerlines over the entire time sequence. However, technical advances in 3D echography, cine-MRI, tagged-MRI and multislice computed tomography (MSCT) devices open today new perspectives. It is now possible to describe the dynamic behavior of the heart over the entire cardiac cycle. MSCT offers in particular a full 3D access to the all cardiac structures, including right and left coronary trees and opens new paths for intra-operative planning capabilities [4][5]. Although promising, a few works have been devoted to motion analysis in MSCT and mainly on left ventricle [6]–[8]. Much less attention has been paid to the estimation of coronary motion. Some studies have been performed on image sequences in bi-plane angiography [3][9][10], EBCT [11] and MRA [12][13]. The only work related to MSCT data [14] relied on manual measurements on the position of bifurcation points.

This paper describes a semi-automatic method to extract the motion of coronary in MSCT volume sequences. It is organized as follows. The methodology designed to extract the coronary networks and their pairing by a point matching algorithm is described in section 2. The experiments conducted on several volume sequences are then presented in section 3. Discussion and perspectives are provided in conclusion.

Methodology

Coronary tree extraction and representation

The coronary centerlines are first extracted by using a tracking-based algorithm proposed in our previous work [15]. It is based on a local cylinder model that provides the vessel position, local contrast, its orientation and diameter. The tracking procedure is initialized by manually selecting seed points (lying on targeted vessels). The centerline point and local diameter is estimated by geometric moment-based operator. A multiscale approach [16] has been used to handle highly varying vessel diameters and criterions have been proposed to deal with branching and end points. To represent the extracted vessels, we introduce a N -tuple vector for each centreline point that may gather vascular features, including the 3D space coordinates and the local intensity, diameter, direction, etc. This point-based attributed vector is denoted as $\mathbf{x} = [x_1, \dots, x_N]^T$ (where the prime means the vector or matrix transpose). For the coronary tree at cardiac phase t , we define $X_t = \{\mathbf{x}_i, i=1, \dots, n_t\}$ as the related attributed point set (with n_t the total number of points). Then, a total of K dynamic volumes provide a sequence of dynamic point sets $\{X_t, t=0, \dots, K-1\}$ that characterizes the temporal and spatial behavior of the coronary tree.

Constrained point-based matching

We assume that the point set X_t relates to a point set X_{t+1} by a mapping $\varphi_t(\mathbf{x}): \mathbb{R}^N \mapsto \mathbb{R}^N$. Then, a global motion of coronary tree might be established by solving a group of mappings $\{\varphi_t\}$. In this paper, we have limited our study to the B-spline based parametric φ which can be expressed as

$$\varphi(\mathbf{x}) = \mathbf{x} + \begin{bmatrix} \sum_{\ell=1}^{L_1} c_{1\ell} b_{1\ell}(\mathbf{x}) \\ \vdots \\ \sum_{\ell=1}^{L_N} c_{N\ell} b_{N\ell}(\mathbf{x}) \end{bmatrix}$$

with $\{b_{n\ell}(\mathbf{x})\}_{n=1, \ell=1}^{L_n}$ representing the cubic B-spline basis functions for the n th Cartesian direction, and $\{c_{n\ell}\}_{n=1, \ell=1}^{L_n}$ the corresponding unknown coefficients, where n, L_n represent the dimensions of attribute points and the number of control points on the n th dimension respectively. This parametrization is very popular in image registration and suitable for modeling the nonrigid local movement. For conciseness, let us define $P: \{p_i = \{p_{i,1}, \dots, p_{i,n}\}\}_{i=1}^I$ and $Q: \{q_j = \{q_{j,1}, \dots, q_{j,n}\}\}_{j=1}^J$ as the generalized target and source attributed point sets. Then, when estimating φ_t , we let P equal to X_t and Q equal to X_{t+1} . This avoids repeated notations. We further suppress the subscript t of φ_t to denote φ for simplicity.

However, the estimation of the mapping φ is nontrivial since 1) even in an ideal situation, because the points are independently extracted from different cardiac volumes, a one-to-one relationship between X_t and X_{t+1} can not be assumed; 2) in real case, the possible loss of parts of vascular segments (due to contrast variations, reconstruction artifacts, etc.) must be considered: thus, subsets of attributed points can be missing and will not have any pairing in the previous or next volume. As noted by [17], instead of a hard one-to-one mapping, we suppose that a source point can be assigned to all target points with a certain probability. This results in the so-called soft-assign, i.e., the correspondence between points \mathbf{p}_i and \mathbf{q}_j is measured by an additional parameter w_{ij} where $0 \leq w_{ij} \leq 1.0, \forall i, j$, and $\sum_j w_{ij} = 1.0$ (for $i = 1, \dots, I$, which ensures that $\{w_{ij}\}$ form a valid probability distribution). Such w_{ij} 's therefore should be resolved together with the mapping φ .

A particular feature of the object (i.e., coronary network) is that its topology does not change under motion. Thus, branching (or bifurcation) and ostium points can be seen as stable landmarks onto which the pairing can rely. Establishing such relations is highly important and has to be considered in the construction of an accurate dynamic tree tracking. So, these landmark points are distinguished by defining the sets P and Q in which the m th point $\tilde{\mathbf{p}}_m$ in P matches the m th point $\tilde{\mathbf{q}}_m$ in Q . In the following, this prior knowledge will be used to develop a specific regularization for motion estimation. To sum up, the desired mapping, including unknown correspondences, can be achieved by minimizing

$$\Psi(\{c_{n\ell}\}, \{w_{ij}\}) = E_1(P, Q; \{c_{n\ell}\}, \{w_{ij}\}) + \alpha E_2(\tilde{P}, \tilde{Q}; \{c_{n\ell}\}) + \beta R_1(\{c_{n\ell}\}) + \gamma R_2(\{w_{ij}\})$$

with respect to $\{c_{n\ell}\}$ and $\{w_{ij}\}$, subject to $0 \leq w_{ij} \leq 1.0$ ($\forall i, j$) and $\sum_j w_{ij} = 1.0$ ($\forall i$) where α, β , and γ are adjustable parameters.

The first right-hand-side term of (2) is the figure of merit measuring the similarity between target point set and the deformed source point set. It is defined by

$$E_1(P, Q; \{c_{n\ell}\}, \{w_{ij}\}) = \frac{1}{2} \sum_{i=1}^I \sum_{j=1}^J w_{ij} \|\mathbf{p}_i - \varphi(\mathbf{q}_j)\|^2$$

where $\|\cdot\|$ is the Euclidean norm. The second term regularizes the landmarks pairings and has the form

$$E_2(\tilde{P}, \tilde{Q}; \{c_{n\ell}\}) = \frac{1}{2} \sum_{m=1}^M \|\tilde{\mathbf{p}}_m - \varphi(\tilde{\mathbf{q}}_m)\|^2.$$

It forces any selected source feature point $\tilde{\mathbf{p}}_m$ to be as consistent as possible with its target pair $\tilde{\mathbf{q}}_m$.

The term $R_1(\{c_{n\ell}\})$ is the smoothing penalization term for the mapping φ . Here, we consider the discrete Markov random field (MRF) so that the penalty can be written

$$R_1(\{c_{n\ell}\}) = \frac{1}{2} \sum_n \sum_{\ell} \sum_{s \in \partial \ell} r_{\ell s} (c_{n\ell} - c_{ns})^2$$

where $\partial \ell$ denotes the usual second-order neighborhoods of the B-spline control point ℓ , and $r_{\ell s}$ is the reciprocal distance between control point ℓ and s .

The last term $R_2(\{w_{ij}\})$ penalizes the correspondence w_{ij} 's. Since one source point must be assigned to one target point with relatively larger probability, it can be expected that $\{w_{ij}\}$ (for a fixed i) should have a peak around certain point (as well as j) forming a narrowed distribution. Thus, a good choice to impose such prior information is to use the entropy as it was recommended by [17]:

$$R_2(\{w_{ij}\}) = \sum_{i=1}^I \sum_{j=1}^J w_{ij} \log w_{ij}.$$

Another interesting advantage for this penalty is that, when performing iterative optimization, the update for w_{ij} has a closed form expression that automatically fulfills the required nonnegativity constraints. Finally, we solve the optimal $\{c_{n\ell}\}$ and $\{w_{ij}\}$ of each two consecutive phases t and $t + 1$ using the alternating minimization algorithm.

Model reconstruction

Once $\{\varphi_t\}$ have been solved, we are able to track the movement of each point of centerlines throughout the overall cardiac cycle. More precisely, given a point $\mathbf{x}_{0,i} \in \{X_0\}$, we can find out its spatial locations as $\{\varphi_0(\mathbf{x}_{0,i}), \varphi_1(\varphi_0(\mathbf{x}_{0,i})), \dots\}$ for the complete volume image sequence. We then interpolate the all point-based trajectories in order to get a continuous description of the movement. Therefore, any intermediate states of the beating heart within the cardiac cycle can be approximated.

Results and Discussion

Five breath-hold MSCT sequences, acquired on a GE Light Speed VCT 64 multi-detectors scanner, were used to evaluate the method. Each sequence included 10 volumes reconstructed from slices acquired every 10% of the cardiac cycle and on several cycles. The pixel size ranged between 0.30mm and 0.35mm and the slice spacing was equal to 0.625mm. A 3D linear interpolation was systematically carried out on each volume of the sequence to make it isotropic. Then, all the sequences of volumes were processed. We provide, for illustration, the main results for two data sets, acquired on patients having respectively an arterial hypertension (Data 1) and a dilated cardiomyopathy (Data 2). In both cases, the coronary networks were considered as normal. The sizes of the data sets were $512 \times 512 \times 316$ and $512 \times 512 \times 332$ respectively.

Coronary tree extraction

The vessel tracking based on the extraction algorithm is initiated with user-defined seed points (in average, 2 to 6 points are required for extracting the left and right coronary trees). Some additional seed points may be needed when the scene is more complex, i.e. in presence of calcified plaques, or when the contrast is low.

Main arteries, such as left main (LM), left anterior descending (LAD), left circumflex (LCx), diagonals (DI), oblique marginal (OM), right coronary artery (RCA) and posterior descending artery (PDA), were extracted in almost all volume sequences. All branches are structurally defined by ordering their subsets of points (including their branching and end points). A cardiologist verified then the validity and the accuracy of centerlines for each volume of each sequence and labeled them with their anatomical names. For illustration, two centerline trees extracted from the 10% and 20% volumes (Data 1) are plotted together with landmarks in Fig. 1(a).

Generally speaking, the extraction method behaves well on data sets that do not have too many artifacts. These artifacts are mainly due to reconstruction problems either caused by an irregular heart rate or by too fast motions of structures related to the rotation speed of the acquisition system. The latter one mainly occurs in early systolic and end-diastolic phases and can affect 50% of the volumes of the sequence. Motion artifacts introduce blurring effects and a splitting of vessels, making difficult even impossible in some cases their extraction. This has been the case for the right coronary artery (RCA) in some volumes for two of the five sequences [18].

Other difficulties come from the low contrast with the surrounding tissues and its variability which lead to over- or underestimations of vessel diameters and loss of parts of segments over time. This explains why, in a first step, the diameter has been computed only on the volumes reconstructed at the rest phases of the heart (70%, 80% of the cardiac cycle), these ones being exempt of motion artifacts. Extracting the vascular trees may take up to 20 minutes for a whole time sequence, the major part being devoted to interactive seeding (the spatial tracking algorithm being very fast, about several seconds for a branch on a computer P4-3.06G, 1G RAM). The continuous advances of MSCT should provide better resolution and contrast, such that these limitations will be minimized in the next future.

Point Matching

The point sampling over a branch is uniform. We used only the 3D coordinates as attributes for the point matching algorithm, i.e., $N = 3$. As pointed out in Section II-B, the lengths of the branches are not the same all over the sequence due to different terminations of the vessel tracking algorithm. This situation is exemplified by the circle in Fig. 1(a) for small vascular segments. To deal with this length difference, the matching process considers the shortest segment to be paired within the two volumes. This is carried out by using the structural descriptions already available and the fact that the known branching points serve as constraints.

Matching results are shown in Fig. 1(b). We used $L_n = 8^3$, ($n = 1, \dots, 3$) as the coefficient number of B-spline basis functions in each dimension of \mathbf{x} . The parameters in equation (2) were: $\alpha = 3.0$, $\beta = 0.1$ and $\gamma = 0.1$. Their values have been obtained from an training phase carried out on the five data sets. They were selected to minimize the error of matching defined below. The displacements resulting from the source and target pairing for each branch and estimated by φ_t are represented by straight lines. Significant cardiac motions can be observed, especially for RCA. Their magnitudes are spatially and anatomically coherent while varying from proximal to distal segments. In order to get a more quantitative picture, we measured the Euclidean distance between $\varphi\{\mathbf{q}_j\}$ and the target centerlines P by using the rule of comparison the nearest point. The root mean square error (RMSE) is computed as $\sqrt{\frac{1}{J} \sum_{j=1}^J \|\varphi(\mathbf{q}_j) - \mathbf{p}_j\|^2}$ where J is the point number in Q and \mathbf{p}_j is the nearest point for $\varphi(\mathbf{q}_j)$ on the centerlines represented by point set P.

Mean RMSE and 3D displacement have been computed for all the extracted branches in all phases and patients. Considering the non-linear nature of cardiac motion, displacements have been measured separately for each of the coronary branches.

Fig. 2 provides for illustration the mean RMSEs and 3D displacements for the LAD and RCA branches of Data 1 during a cardiac cycle. The value at 0% is used as 100% to have a complete analysis throughout a cardiac cycle. For this sequence, considering the LAD and RCA arteries, the maximum displacement and RMSE during a cardiac cycle are 7.20mm and 1.20mm, 18.07mm and 1.68mm respectively.

If we consider now the whole set of sequences, we found a maximum 3D displacement for LAD that ranges between 5.03mm and 14.50mm with a maximum RMSE comprised between 0.82mm and 2.51 mm according to the considered sequence. For the RCA artery these values are [18.64 – 19.14]mm and [0.91 – 1.69]mm respectively.

3D+t analysis

Two 3D+t coronary trees with a total of 40 volumes are finally generated after interpolation. The vascular networks at four distinct instants are displayed together in Fig. 3 where the vessel diameters are approximated through the moment-based operator at 70% or 80% instants. We have used the landmarks proposed in [19] with an additional one to analyze the dynamic behavior of the beating heart: LM ostium (LM_o), LAD-LCx bifurcation (LM_b), 5cm away from LM_o on LAD (LAD_5), 5cm away from LM_o on LCx (LCx_5), RCA ostium (RCA_o) and RCA-PDA bifurcation (RCA_{PDA}). Fig. 4 provides the spatial evolution of these points over time, taking as reference their positions at 0%. It can be seen that RCA landmarks have larger displacements, and subsequently larger velocities. The maximum displacements are obtained for the time-indexed volumes 40% and 50% corresponding to the end of systole. Three main peaks, located approximately at 20%, 60% and 90% on the velocity curves, represent three main cardiac phases with fast cardiac motion, i.e., systole, diastolic filling and atrial contraction. The first peak representing the systolic period is related to opening and closing of aortic valve throughout the R-R interval illustrated in Fig. 4(c). These results are in accordance with those reported in [14][19].

Conclusion

The main contribution of this short paper is the 3D tracking of the coronary tree over a full cardiac period, which allows studying the beating heart behavior and patterns of individual vascular segments, thus bringing new cues on the corresponding myocardium territories. The matching of centerlines is fully automatic and needs less than 10 minutes on a computer P4-3.06G with 1G RAM. The most critical feature is related to the choice of control parameters (α , β and γ). An intensive exploration of the parameter space has been conducted and the values applied in this paper represent the best compromise we found. A learning stage based on more extensive experiments will be conducted on that point.

The work in progress is devoted on one hand to improve the segmentation step and the local vessel characterization in order to enrich the attributed centreline description and to decrease the time required for processing a complete volume sequence. On the other hand, the robustness of the constrained point matching will be extended to deal with partial correspondence. Lastly, new features of the coronary network (for instance, the overall heart movement, i.e rotation-translation, local shapes and deformations, asynchronous segments) will be derived in order to enrich the set of information for diagnosis.

Acknowledgements:

The authors are indebted to Jean-Louis Coatrieux for his advices all along this research project and the suggestions brought to this manuscript. This work has been supported by a scholarship of the French government.

References:

- 1 . Mackay J , Mensah G . The Atlas of heart disease and stroke . Geneva, Switzerland World Health Organization ; 2004 ;
- 2 . Frangi AF , Niessen WJ , Viergever MA . Three-dimensional modeling for functional analysis of cardiac images: a review . IEEE Trans Med Imag . 20 : (1) 2 - 25 Jan 2001 ;
- 3 . Ruan S , Bruno A , Coatrieux JL . Three-dimensional motion and reconstruction of coronary arteries from biplane cineangiography . Imag Vis Comput . 12 : (10) 683 - 689 1994 ;

- 4 . Shechter G , Shechter B , Resar JR , Beyar R . Prospective motion correction of x-Ray images for coronary interventions . *IEEE Trans Med Imag* . 24 : (4) 441 - 450 Apr 2005 ;
- 5 . Coatrieux JL , Rioual K , Goksu C , Unanua E , Haigron P . Ray casting with "on-the-fly" region growing: 3-D navigation into cardiac MSCT volume . *IEEE Trans Inf Technol Biomed* . 10 : (2) 417 - 420 Apr 2006 ;
- 6 . Song SM , Leahy RM . Computation of 3-D velocity fields from 3-D cine CT images of a human heart . *IEEE Trans Med Imag* . 10 : (3) 295 - 306 Sept 1991 ;
- 7 . Gorce JM , Friboulet D , Magnin IE . Estimation of three-dimensional cardiac velocity fields: assessment of a differential method and application to three-dimensional CT data . *Med Image Anal* . 1 : (3) 245 - 261 Apr 1997 ;
- 8 . Garreau M , Simon A , Boulmier D , Coatrieux JL , Breton HL . Assessment of left ventricular function in cardiac MSCT imaging by a 4D hierarchical surface-volume matching process . *Int J Biomed Imaging* . 1 : (1) 1 - 10 2006 ;
- 9 . Puentes J , Roux C , Garreau M , Coatrieux JL . Dynamic feature extraction of coronary artery motion using DSA image sequences . *IEEE Trans Med Imag* . 17 : (6) 857 - 871 Dec 1998 ;
- 10 . Shechter G , Devernay F , Coste-Maniere E , Quyyumi A , McVeigh ER . Three-dimensional motion tracking of coronary arteries in biplane cineangiogram . *IEEE Trans Med Imag* . 22 : (4) 493 - 503 Apr 2003 ;
- 11 . Achenbach S , Ropers D , Holle J , Muschiol G , Daniel WG , Moshage W . In-plane coronary arterial motion velocity: Measurement with electron-beam CT . *Radiology* . 216 : 457 - 463 Aug 2000 ;
- 12 . Hofman MB , Wickline SA , Lorenz CH . Quantification of in-plane motion of the coronary arteries during the cardiac cycle: implications for acquisition window duration for MR flow quantification . *J Magn Reson Imaging* . 8 : (3) 568 - 576 May-June 1998 ;
- 13 . Saranathan M , Ho VB , Hood MN , Foo TKF , Hardy CJ . Adaptive vessel tracking: automated computation of vessel trajectories for improved efficiency in 2D coronary MR angiography . *J Magn Reson Imaging* . 14 : (4) 368 - 373 2001 ;
- 14 . Husmann L , Leschka S , Desbiolles L , Schepis T , Gaemperli O , Seifert B , Cattin P , Frauenfelder T , Flohr TG , Marincek B , Kaufmann PA , Alkadhi H . Coronary artery motion and cardiac phases: dependency on heart rate implications for CT image reconstruction . *Radiology* . 245 : (2) 567 - 576 Nov 2007 ;
- 15 . Yang G , Bousse A , Toumoulin C , Shu H . A multiscale tracking algorithm for the coronary extraction in MSCT angiography . *Proc. IEEE EMBS 2006* ; 1 : New York, NY, USA Aug. 2006 3066 - 3069
- 16 . Frangi AF , Niessen WJ , Vincken KL , Viergever MA . Multiscale vessel enhancement filtering . *Lecture Notes in Computer Science* . 1496 : Medical Imaging Computing & Computer-Assisted Intervention 130 - 137
- 17 . Chui H , Rangarajan A . A new point matching algorithm for non-rigid registration . *Comput Vis Image Und* . 89 : (2-3) 114 - 141 2003 ;
- 18 . Greuter MJW , Dorgelo J , Tukker WGJ , Oudkerk M . Study on motion artifacts in coronary arteries with an anthropomorphic moving heart phantom on an ECG-gated multidetector computed tomography unit . *Eur Radiol* . 15 : (5) 995 - 1007 May 2005 ;
- 19 . Shechter G , Resar JR , McVeigh ER . Displacement and velocity of the coronary arteries: cardiac and respiratory motion . *IEEE Trans Med Imag* . 25 : (3) 369 - 375 Mar 2006 ;

Figure 1

(a) Centerline extraction results for the 10% (red) and 20% (blue) volumes of Data1. The centerlines are depicted by their coordinates in the volumes. Symbols mark the ostia and bifurcations. The circle shows truncated branches. (b) Pairing results when matching the two centerline sets of 10% (red) with the centerlines of 20% (blue) in (a). The movement relations are displayed by black lines.

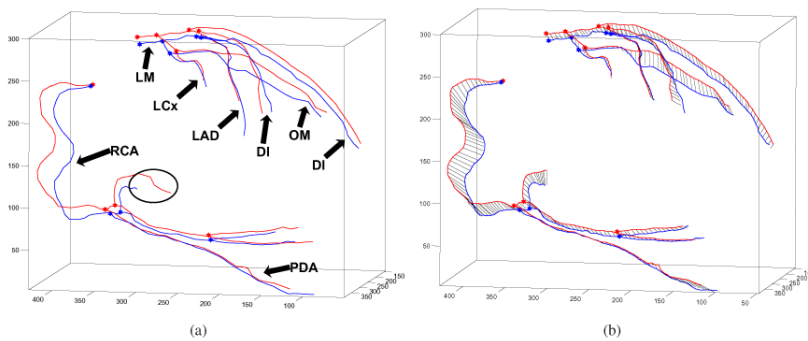


Figure 2

Mean 3D displacements() and RMSEs of point matching(•) for LAD(a) and RCA(b) from Data 1. 3D displacements and RMSEs are calculated between every two 10 % R-R intervals. The error bars show the standard deviations of 3D displacements.

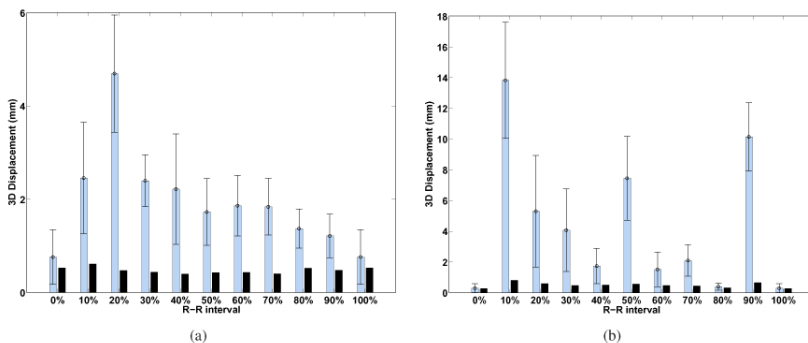


Figure 3

3D+t coronary tree models reconstructed from Data1(a) and Data2(b) at four instants during a R-R interval, i.e. 0%(), 20%(), 40%() and 80%().

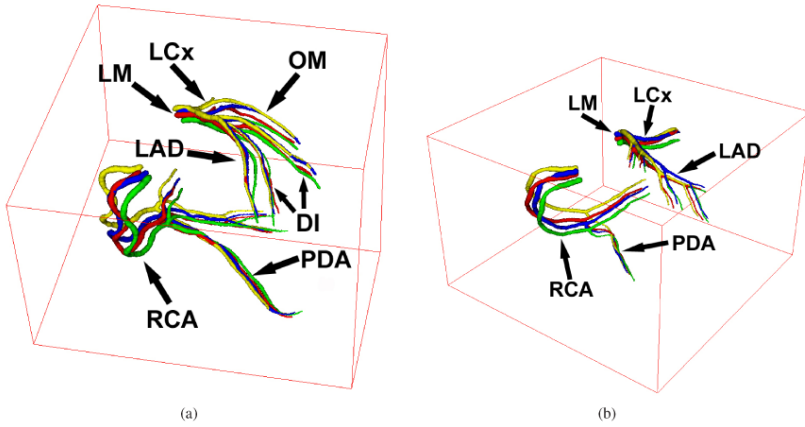


Figure 4

3D displacement(a) away from the position at 0% at each instant and velocity(b) for the landmarks LM_0 , LM_B , LAD_5 , LCx_5 , RCA_0 and RCA_{PDA} in Data2. Opening and closing of aortic valve(c) throughout R-R interval show the systolic period marked by red box.

